Title

Universal Dynamics of Molecular Reorientation in Hybrid Lead Iodide Perovskites

Journal

Journal of the American Chemical Society, 139(46)

ISSN

0002-7863 1520-5126

Authors

Fabini, Douglas H
Siaw, Ting Ann
Stoumpos, Constantinos C
et al.

Publication Date

2017-11-02

DOI

10.1021/jacs.7b09536

Peer reviewed

Universal Dynamics of Molecular Reorientation in Hybrid Lead Iodide Perovskites

Douglas H. Fabini,[†] Ting Ann Siaw,[‡¤] Constantinos C. Stoumpos,[¶] Geneva Laurita,[§] Daniel Olds,[‖] Katharine Page,[‖] Jerry G. Hu,[†] Mercouri G. Kanatzidis,[¶] Songi Han,[‡,⊥] and Ram Seshadri[*,†,‡]

[†]*Materials Department and Materials Research Laboratory*
University of California, Santa Barbara, California 93106, United States

[‡]*Department of Chemistry and Biochemistry*
University of California, Santa Barbara, California 93106, United States

[¶]*Department of Chemistry and Argonne-Northwestern Solar Energy Research Center*
Northwestern University, Evanston, Illinois 60208, United States

[§]*Chemistry Department, Bates College, Lewiston, Maine 04240, United States*

[‖]*Spallation Neutron Source, Oak Ridge National Laboratory*
Oak Ridge, Tennessee 37831, United States

[⊥]*Department of Chemical Engineering*
University of California, Santa Barbara, California 93106, United States

E-mail: seshadri@mrl.ucsb.edu

[¤]Current institution: JEOL USA Inc., Peabody, MA 01960, United States

Abstract

The role of organic molecular cations in the high-performance perovskite photovoltaic absorbers, methylammonium lead iodide ($MAPbI_3$) and formamidinium lead iodide ($FAPbI_3$), has been an enigmatic subject of great interest. Beyond aiding in the ease of processing of thin films for photovoltaic devices, there have been suggestions that many of the remarkable properties of the halide perovskites can be attributed to the dipolar nature and the dynamic behavior of these cations. Here, we establish the dynamics of the molecular cations in $FAPbI_3$ between 4 K and 340 K and the nature of their interaction with the surrounding inorganic cage using a combination of solid state nuclear magnetic resonance and dielectric spectroscopies, neutron scattering, calorimetry, and ab initio calculations. Detailed comparisons of the reported temperature dependence of the dynamics of $MAPbI_3$ are then carried out which reveal the molecular ions in the two different compounds to exhibit very similar rotation rates ($\approx$8 ps) at room temperature, despite differences in other temperature regimes. For FA, rotation about the N···N axis, which reorients the molecular dipole, is the dominant motion in all phases, with an activation barrier of $\approx$21 meV in the ambient phase, compared to $\approx$110 meV for the analogous dipole reorientation of MA. Geometrical frustration of the molecule–cage interaction in $FAPbI_3$ produces a disordered γ-phase and subsequent glassy freezing at yet lower temperatures. Hydrogen bonds suggested by atom–atom distances from neutron total scattering experiments imply a substantial role for the molecules in directing structure and dictating properties. The temperature dependence of reorientation of the dipolar molecular cations systematically described here can clarify various hypotheses including large-polaron charge transport and fugitive electron spin polarization that have been invoked in the context of these unusual materials.

Introduction

The behavior of the organic molecular cations in the hybrid organic–inorganic main-group halide perovskites has attracted great attention in recent years, in part because the liquid-like disorder of this sublattice represents something of a novelty with respect to "traditional" semiconductors.[1–4] These dense, hybrid materials are of both fundamental and applied interest. These systems occupy an underexplored region of the space of plastic crystals (which exhibit translational periodicity but orientational disorder)[5–8] between better-studied molecular salts and open 3-D coordination polymers, and are likely to display complex couplings between microscopic, dynamic processes and macroscopic phase transitions. Further, understanding the molecule–cage interaction in these high performance semiconductors with potential optoelectronic applications[9–11] is essential for achieving full compositional control of the different material properties, as well as for the design and discovery of new functional materials.

Since the first preparation of the hybrid lead halide perovskites,[12] the behavior of the molecular cations has been studied by calorimetry,[13,14] infrared spectroscopy,[13,15,16] dielectric spectroscopy,[14,17–20] Raman spectroscopy,[21] quasi-elastic and inelastic neutron scattering,[22–26] nuclear magnetic resonance (NMR) spectroscopy,[27–32] isotopic substitution,[33] and ab initio methods,[34–39] and these findings have been correlated to the structure evolution from crystallographic techniques.[19,40–46] Most of these efforts have focused on MAPbX_3 (methylammonium lead halides; MA = CH_3NH_3, X = Cl, Br, I). In contrast, reports on $FAPbI_3$ (formamidinium lead iodide; FA = $CH[NH_2]_2$) have been less prolific, and understanding of the system remains incomplete in spite of the highly appealing photovoltaic performance of compounds with the formamidinium ion.[11]

The molecular cations have at times been invoked to explain all manner of confounding phenomena observed in these remarkable materials, including facile charge separation,[47] a high tolerance to intrinsic point defects,[48] persistent hot carriers,[49] and possible dynamic spin-splitting of the band extrema.[50] These hypotheses are somewhat misaligned with the

growing body of evidence suggesting an important role for local distortions of the inorganic sublattice.[22,51–59] Indeed, there are now numerous indications that the appealing optoelectronic properties of the hybrid perovskites are qualitatively matched by their all-inorganic analogues.[54,60–64]

In order then to delineate the properties and functionality of the molecular cations from those of the inorganic framework, one must first complete the description of the structure and dynamics of each. To this end, we employ solid-state NMR, a technique which is proved crucial for the study of plastic crystals.[5,27–29,65–70] We complement the studies with neutron scattering, dielectric spectroscopy, calorimetry, and ab initio calculations to establish the behavior of the formamidinium ion and its coupling to the lattice in $FAPbI_3$ between 4 K and 340 K. Despite differences above and below room temperature, $FAPbI_3$ and $MAPbI_3$ are seen to exhibit very similar rates of molecular reorientation near 300 K. The unusual reentrant β–γ phase transition at 140 K reported in $FAPbI_3$[19] is revealed to be a cascade of processes over a narrow temperature window, despite rather smoothly varying rotational dynamics. Below 100 K, molecular motion slows considerably, but the molecular geometry appears to be incompatible with the preferred ground state octahedral tilting pattern of the inorganic framework, leading to disordered freezing. Temperature-dependent pair distribution functions from neutron scattering suggest hydrogen bonds from the amine groups to the iodines of the surrounding cage, highlighting the role of the molecule in directing structure and modifying lattice dynamics and electron–phonon interaction. This work establishes important structural and dynamical details necessary for the evaluation of emerging hypotheses regarding the possible role of the molecular cations in the unusual and appealing optoelectronic properties of these hybrid materials.

Results & Discussion

Solid state ^{1}H nuclear magnetic resonance (NMR) spin-lattice relaxation time (T_1) experiments were conducted at temperatures between 4 K and 340 K. 1-D spectra and relaxation times from 10 kHz magic-angle spinning (MAS) experiments above 220 K (ω_0 = 500 MHz) are presented in Figure 1 (spectra for the yellow hexagonal δ-phase are provided in the supporting information in Figure S1 for comparison). Due to the strong dipolar interactions associated with ^{1}H, it is not possible to resolve the three chemically distinct protons under achievable MAS speeds, as in an equivalent solution-state experiment.[43] As expected, the changes in the spectra with temperature are subtle, reflecting only temperature effects on spin polarization, slight broadening, and gradual changes in chemical shift. By fitting a single pseudo-Voigt function to the central peak (which comprises features from each of the chemically distinct protons, broadened by dipolar interactions and chemical shielding anisotropy), we observe that the protons become slightly more shielded on cooling (Figure 1c), consistent with lattice contraction and increased residence time near the electron-rich iodides of the inorganic cage as molecular motion slows.

The peak shape and T_1 are extremely sensitive to the onset of the otherwise subtle continuous α–β phase transition near 275 K (Figure 1d–e). The line broadening in the tetragonal β-phase suggests that molecular motions become anisotropic, consistent with the reduced site symmetry from X-ray diffraction.[19] Finally, we observe a hastening of spin-lattice relaxation due to critical fluctuations in the vicinity of the transition.

1-D spectra from cryogenic experiments (ω_0 = 300 MHz) at selected temperatures between 4 K and 245 K are presented in Figure 2a. Absorption lines are extremely broad as MAS was not possible with this configuration. Increased shielding is observed on cooling (smaller apparent chemical shift changes are not significant owing to the challenge of precisely phase correcting such broad features), again consistent with lattice contraction and increased residence time of the protons near the electron-rich iodides of the inorganic cage as molecular motion slows. Lineshapes are very similar down to roughly 100 K, confirming

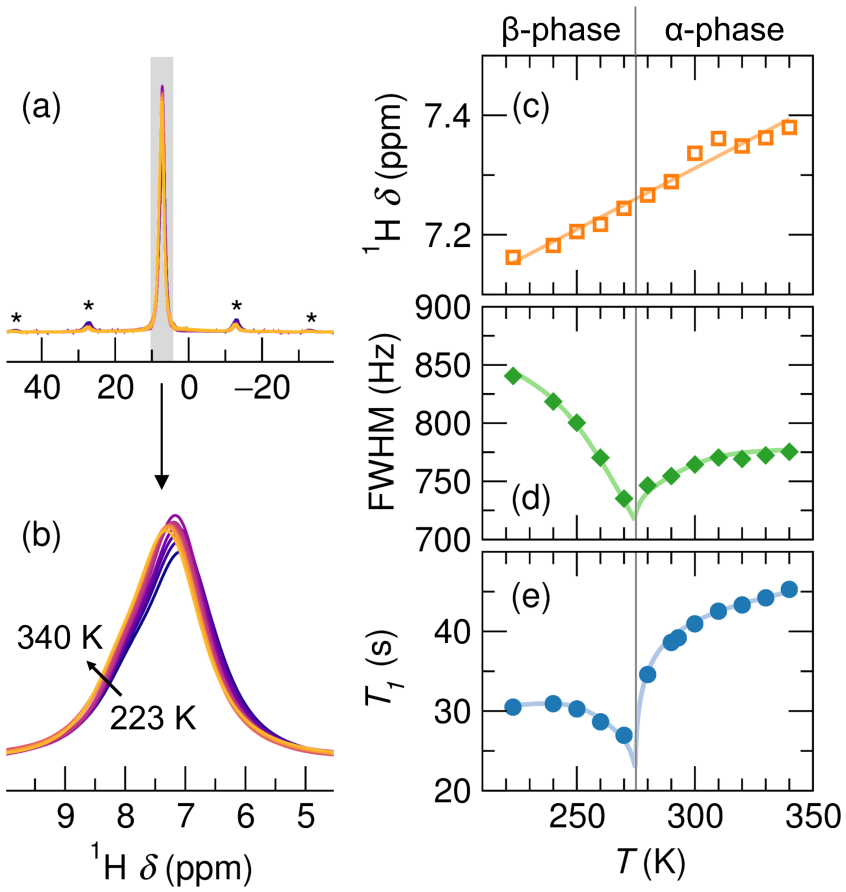

Figure 1: (a,b) Solid state ^{1}H NMR (10 kHz MAS) spectra of perovskite $FAPbI_3$ at temperatures near ambient. Asterisks indicate spinning sidebands. (c) Chemical shift and (d) peak width (full width at half maximum, FWHM) when the data are fit with a single pseudo-Voigt function. (e) Spin-lattice relaxation time (T_1) from inversion recovery experiments. The α–β phase transition is indicated. For (c-e), lines are to guide the eye only, and error bars are smaller than the markers and are omitted for clarity.

that the molecule retains considerable motion into the disordered γ-phase,[19] unlike in the corresponding orthorhombic γ-phase phase of $MAPbI_3$.[41] Below 100 K, the signal broadens considerably as motion becomes too slow to average out dipolar interactions and chemical shielding anisotropy. Due to the presence of a small impurity of the yellow δ-$FAPbI_3$ polymorph detected after the cryogenic experiments, we cannot interpret conclusively the additional lineshape structure that emerges at 60 K and below. This impurity phase was accounted for in the extraction of spin-lattice relaxation times via a constrained fitting routine as detailed in the Methods section.

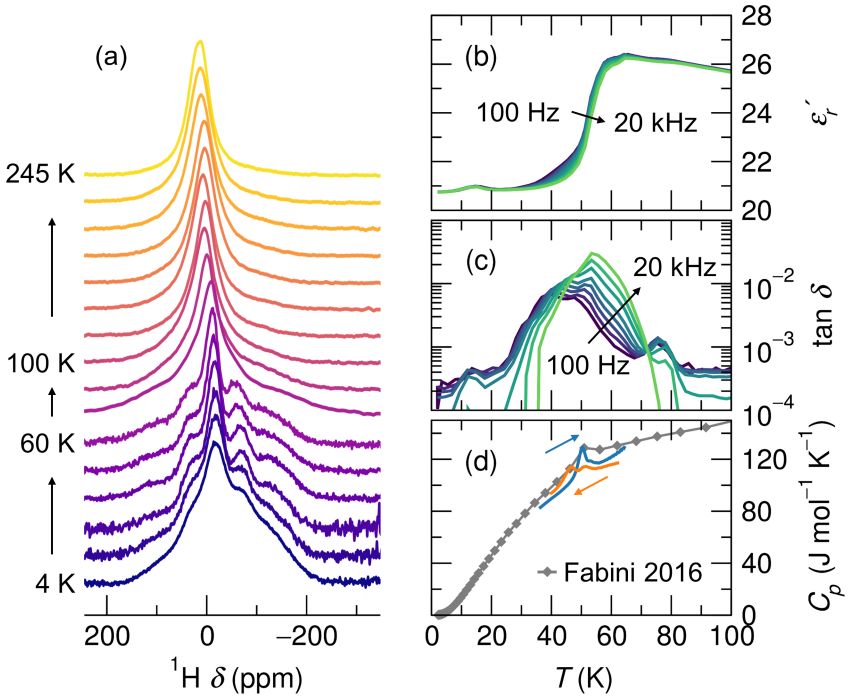

Figure 2: (a) Solid state ^{1}H NMR spectra of perovskite $FAPbI_3$ at selected cryogenic temperatures. (b) Real permittivity (ϵ_r') and (c) loss tangent ($\tan\delta$) from AC capacitance measurements. (d) Heat capacity (C_p) in the vicinity of the freezing of the molecular dipole from rapid warming (blue) and cooling (orange) sweeps, with prior measurements at fixed temperatures from the literature for comparison.[14] Detailed calorimetry and entropy analysis is provided in the supporting information, Figure S2.

The motional slowing of the molecular cation suggested by the broadening of the NMR signal below 100 K is corroborated by dielectric spectroscopy and calorimetry, shown in Figure 2b–d. For the frequencies measured (100 Hz to 20 kHz) the static dielectric con-

stant, ϵ'_r, drops substantially over a ≈25 K temperature window as the dipolar axis of the formamidinium cation is restricted from reorienting. Concurrently, the dielectric loss tangent, tan δ, exhibits frequency-dependent peaks as the frequency of the AC probe resonates with the timescale of dielectric relaxation.[71] This glassy freezing of dipolar motion on cooling is in accordance with our prior report,[14] and in contrast with the abrupt loss of dipolar motion observed in dielectric measurements of $MAPbI_3$ at the β–γ transition.[14,17,18,20] Calorimetry about the motional freezing temperature reveals two closely spaced peaks in the heat capacity, C_p, with a total transition entropy too small to be that of an abrupt order–disorder transition (details in the supporting information, Figure S2), suggesting a gradual loss of motion precedes the phase transition on cooling.

^{1}H spin-lattice relaxation times in $FAPbI_3$, as well as those reported for $MAPbI_3$,[29] are displayed in Figure 3. For both compounds, excluding the known phase transitions, T_1 decreases on cooling until reaching a minimum, and subsequently increases on further cooling. This general temperature-dependence is consistent with relaxation of nuclear spins to the bath by dipole–dipole interactions that fluctuate due to molecular motion.

For $FAPbI_3$, the β–γ transition appears to be characterized by a small but abrupt increase in T_1 over a narrow temperature range (≈135 K to 138 K). Though this would seem to suggest a first-order transition as suggested previously,[14,19] differential scanning calorimetry and relaxation calorimetry (Figure S3) indicate that the transition is in fact a cascade of multiple events with no noticeable hysteresis, and a total transition entropy that is far too small to be a full order–disorder transition. This highlights the unusual nature of this reentrant disordered γ-phase with cubic pseudosymmetry,[19] and points to a more complex molecule–cage interaction in $FAPbI_3$ than in $MAPbI_3$, as suggested previously.[14]

Similarly, the behavior below 100 K is also more complex than that of $MAPbI_3$. Though scattering or complementary spectroscopies will be required to fully elucidate the structure and dynamics in this regime, we note that the intricate temperature-dependence of T_1 is consistent with the multiple sets of dielectric loss peaks observed above, the greater

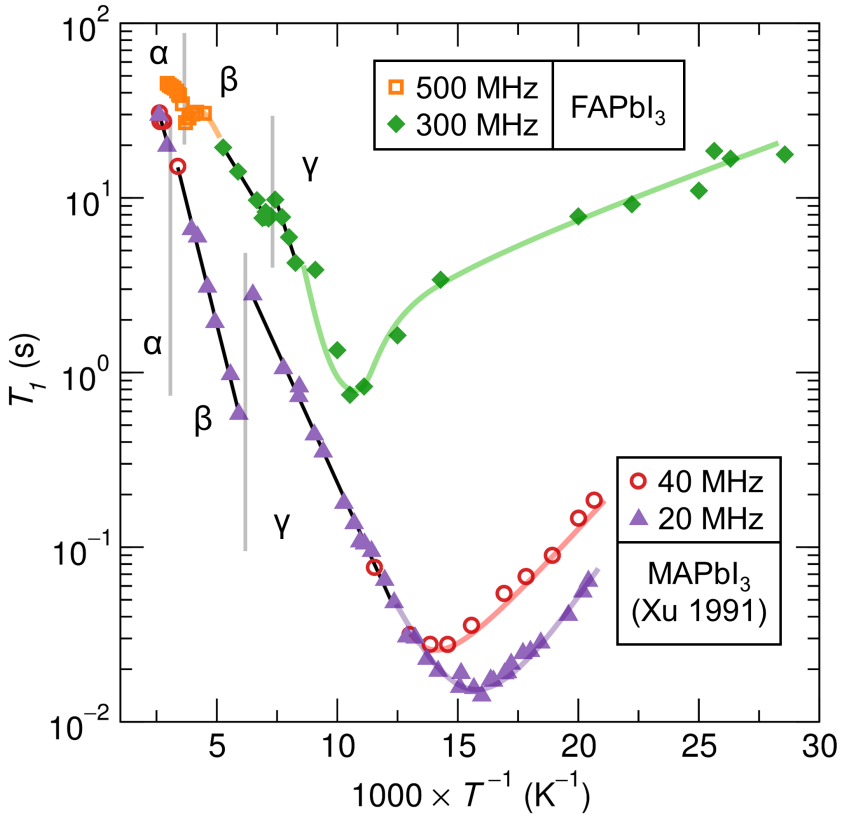

Figure 3: Temperature-dependence of ^{1}H spin-lattice relaxation times (T_1) for $FAPbI_3$, with those reported for $MAPbI_3$ for comparison.[29] Temperature ranges for the α-, β-, and γ-phase of each compound are indicated, and phase transitions are indicated by vertical gray lines. Black lines are Arrhenius fits for activation barriers in each phase. Colored lines are to guide the eye only. For $FAPbI_3$, error bars are smaller than the markers and are omitted for clarity.

fragility of the glassy freezing for this composition,[14] and the predictions of frustrated ground states.[35,36]

The temperature-dependence of T_1 for $MAPbI_3$ is discussed at length in the original report.[29] Notably, there is a significant jump in T_1 on cooling to the γ-phase, which reflects a change in relaxation mechanism as the four-fold rotation about an axis perpendicular to the C–N bond is frozen out, but three-fold rotation about the C–N bond remains.[23,41]

The framework of Bloembergen, Purcell, and Pound[72] has been widely used to interpret T_1 for solids wherein relaxation occurs by dipole–dipole interactions mediated by molecular motions involving the relevant nuclei. In such systems, the predicted T_1 is given in Equation 1, where $C = (3\mu_0^2\hbar^2\gamma^4)/(160\pi^2 r^6)$ is a lumped constant independent of correlation time and field strength. τ_c is the correlation time for molecular motion (the time to rotate through one radian), ω_0 is the Larmor frequency of the nucleus, μ_0 is the vacuum permeability, $\hbar$ is reduced Planck's constant, γ is the gyromagnetic ratio of the nucleus, and r is the dipole–dipole separation distance.

$$\frac{1}{T_1} = C\left[\frac{\tau_c}{1+\omega_0^2\tau_c^2} + \frac{4\tau_c}{1+4\omega_0^2\tau_c^2}\right] \tag{1}$$

In the "fast motion" limit ($\omega_0\tau_c \ll 1$), Equation 1 reduces to $\tau_c = (1/5C)T_1^{-1}$, so activation barriers, E_a, for molecular motion (assuming $\tau_c \approx \exp[-E_a/(k_B T)]$) may be extracted directly from the slopes in Figure 3. The activation barriers for the various phases of both compounds from ^{1}H NMR T_1 measurements are provided in Table 1, as well as those we predict from ab initio calculations of the energy surfaces for molecular rotations in $FAPbI_3$ (Figure 4, vide infra). Somewhat remarkably, given the simplifications made in modeling this high-dimensional problem (vide infra), the barriers we calculate are in excellent agreement with those from experiment for the α- and β-phases of $FAPbI_3$, though we cannot rule out the possibility of a fortuitous cancellation of errors. The underestimate of the activation barrier in the reentrant, pseudo-cubic γ-phase is consistent with our prior finding that the relatively high symmetry and small octahedral tilt angle apparent from

crystallographic studies masks substantial local tilting disorder in this regime[19] which was not included in periodic DFT calculations.

Table 1: Activation barriers (meV) for molecular rotation from ^{1}H NMR (exp.) and DFT (calc.) in the perovskite phases of $FAPbI_3$ and $MAPbI_3$. For all phases of $FAPbI_3$, the rotation is about an axis parallel to the N···N line (ϕ_3 rotations, by the notation of Figure 4). The behavior for $MAPbI_3$ is non-monotonic due to the change in relaxation mechanisms from four-fold rotations (α-, β-phases) to three-fold rotations about C–N (γ-phase).

	α-phase	β-phase	γ-phase
$FAPbI_3$ (exp.)	21	45	84
$FAPbI_3$ (calc.)	21	39	63
$MAPbI_3$ (exp.)[29]	95	110	60

Ab initio energy surfaces for molecular rotations in the perovskite phases of $FAPbI_3$ are displayed in Figure 4. Each curve represents a two-dimensional study of rigid translation and rotation of the molecule (no relaxation of atomic coordinates or unit cell parameters is permitted), but only the locus of points forming the minimum energy path is displayed. Rotations are about the three principal axes of a coordinate system fixed to the molecule, and the structures of the inorganic cage are fixed to those from experiment.[19] Van der Waals corrections are not included.

Barriers to all rotation modes are lowest in the cubic phase, and are sensitive to both lattice parameters and the degree of octahedral tilting. Rotations about an axis parallel to the N···N line (ϕ_3 axis) are the preferred mode in all phases, in agreement with a recent report of heterogeneous dynamics at 300 K from ab initio molecular dynamics.[36] As shown in Table 1, the activation barriers for ϕ_3 rotations are in remarkable agreement with experiment for the α- and β-phases, and a slight underestimate of the experimental value for the disordered γ-phase. Though a few meV higher in energy than the $\phi_1 = 0^\circ$ orientation, the $\phi_1 = 90^\circ$ nominal orientation significantly reduces barrier heights for ϕ_2 and ϕ_3 rotations, suggesting this configuration may be entropy stabilized. This hypothesis is corroborated by charge density analysis of X-ray diffraction experiments (Figure S4).

Figure 5 shows the reorientation times for molecular motion, τ_{rot}, that result from fit-

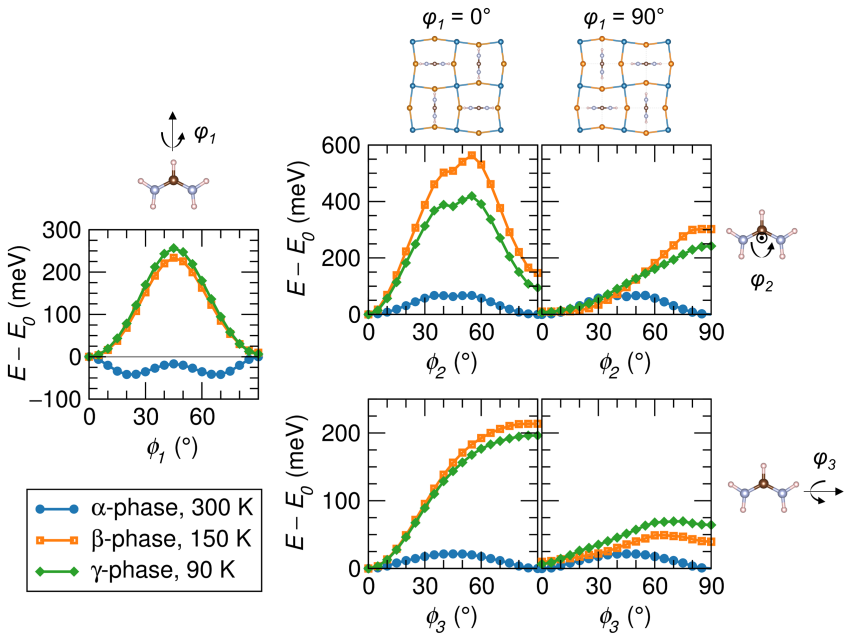

Figure 4: Lowest energy paths for molecular rotations in the three known perovskite phases of $FAPbI_3$, from density functional theory (DFT). Each curve represents a two-dimensional study of rigid translation and rotation of the molecule, but only the locus of points forming the minimum energy path are displayed. Energies are per formula unit. For each rotation mode about the principal axes of the molecule, the other two rotation angles are fixed (for ϕ_1 rotations, $\phi_2 = \phi_3 = 0$; for ϕ_2 rotations, $\phi_1 = (0,\, 90°)$, $\phi_3 = 0$; for ϕ_3 rotations, $\phi_1 = (0,\, 90°)$, $\phi_2 = 0$).

ting the ^{1}H spin-lattice relaxation times for $FAPbI_3$ and $MAPbI_3$[29] within the framework described by Bloembergen, Purcell, and Pound.[72] Estimates of the dynamics reported from a number of other techniques are shown for comparison. Correlation times from fitting T_1 experiments, τ_c, are multiplied by the angle of rotation of the corresponding mode (e.g. $\pi/2$ for the four-fold rotations in α- and β-$MAPbI_3$) to obtain τ_{rot}. Note that some ambiguity remains in defining a consistent reorientation time across these various techniques.

The large discontinuity in τ_{rot} for $MAPbI_3$ at 165 K reflects the loss of four-fold molecular rotation in the orthorhombic γ-phase, as discussed above. For $MAPbI_3$, reorientation times from quasi-elastic neutron scattering over a wide energy-transfer and momentum-transfer range (5 ps at RT) are in general agreement with those from ^{1}H NMR (7 ps at RT) over much of the temperature range,[23] while those from a more limited experimental window estimate a slightly larger τ_{rot} at room temperature (14 ps).[24] For both compounds, room temperature estimates from ab initio molecular dynamics (2 ps to 4.3 ps)[16,36,41] are somewhat shorter than those from ^{1}H NMR (FA: 8 ps; MA: 7 ps). Among reported values, the estimate of τ_{rot} for $MAPbI_3$ from ^{14}N NMR experiments via a diffusion-on-a-cone model (108 ± 18 ps)[73] is an outlier.

It appears that despite rather different energetic barriers for molecular motion in the two compounds, $FAPbI_3$ and $MAPbI_3$ coincidentally exhibit very similar rotational dynamics near room temperature. Above the glassy freezing in $FAPbI_3$ ($\approx$50 K) and above the β–γ transition in $MAPbI_3$ (165 K), these reorientation times are associated with modes that reorient the dipole axis of the molecules, which are intimately linked to dielectric properties, local electric fields, and dynamic symmetry-breaking. The coincident room temperature dynamics observed here in the two compounds suggest a need for further study of the molecular contribution to the full frequency-dependent dielectric response. With one exception,[15] reports in this area appear to be limited to ab initio calculation of the molecular dipole moments (MA: 2.3 D; FA: 0.2 D)[47] and to electrical[14,17–20] and optical[74] measurements of dielectric response which are far slower or far faster, respectively, than molecular

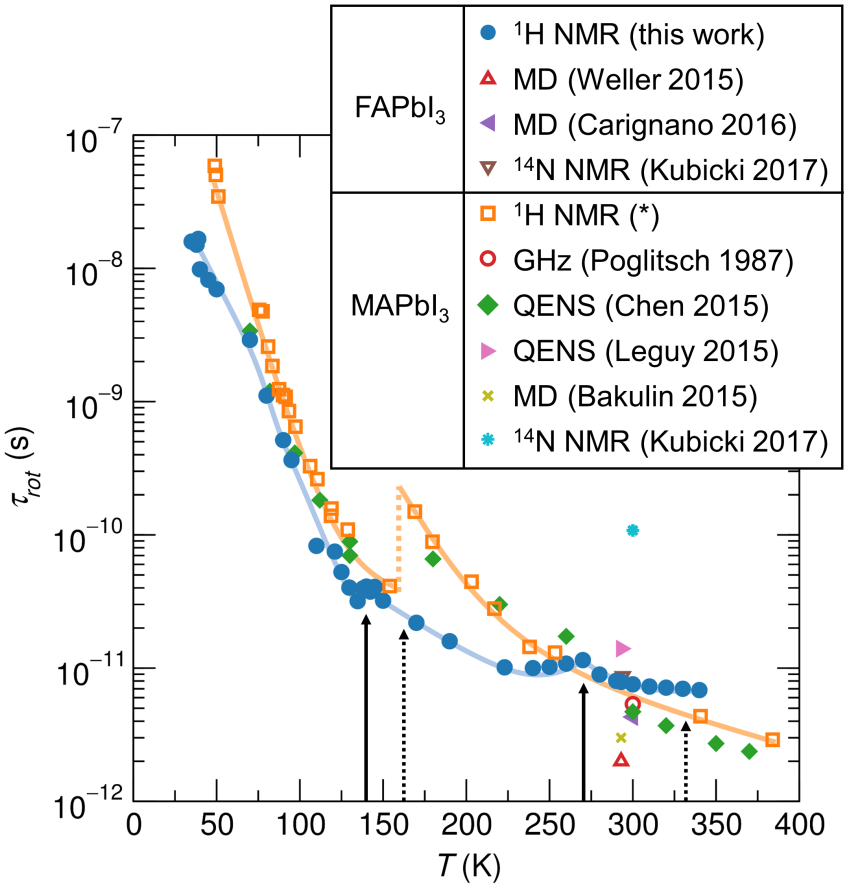

Figure 5: Temperature-dependence of the molecular reorentation time (τ_{rot}) in $FAPbI_3$ and $MAPbI_3$ modeled from ^1H T_1 using the model of Bloembergen, Purcell, and Pound.[72] Phase transition temperatures are indicated by solid ($FAPbI_3$) and dashed ($MAPbI_3$) arrows. Colored lines are to guide the eye only. (*) ^1H T_1 data for $MAPbI_3$ are taken from Xu and coworkers.[29] Reported reorientation times from GHz spectroscopy, quasi-elastic neutron scattering (QENS), ab initio molecular dynamics (MD), and ^{14}N NMR are presented for comparison.[15,16,23,24,36,42,73]

reorientation. In particular, it is intriguing to consider if the differing barriers to molecular dipole rotation and differing dipole moments lead to important differences between $FAPbI_3$ and $MAPbI_3$ on timescales relevant to exciton dissociation, interaction of charge carriers with polar optical phonons or polarons, or momentum separation of excited electrons and holes due to possible dynamic Rashba–Dresselhaus effects.

Near room temperature (where T_1 is independent of field strength), the longer relaxation times in $FAPbI_3$ compared with $MAPbI_3$ despite similar dynamics suggest less effective spin-lattice relaxation, perhaps related to the reduced density of ^{1}H nuclei. Indeed, the ratio of the dipole–dipole distances obtained from fitting to the model of Bloembergen, Purcell, and Pound[72] ($r_{FA} = 2.35$ Å; $r_{MA} = 1.90$ Å), is nearly inverse to the ratio of the volumetric number density of H in the two compounds. As a matter of practice, the broad agreement between the results for $MAPbI_3$ from ^{1}H NMR and from QENS, techniques which both probe hydrogen but leverage distinct physics, confers a degree of confidence in our results and suggests the use of these methods for future studies of molecular motion in related compounds.

To further understand the molecule–cage interaction in $FAPbI_3$, we analyzed pair distribution functions at 100 K, 300 K, and 500 K from neutron total scattering experiments on an N-deuterated sample ($CH[ND_2]_2PbI_3$, to reduce the incoherent scattering contribution from ^{1}H). One expects that substitution of D for H may impact the molecular moment of inertia as well as hydrogen bond strengths,[75] possibly modifying the evolution of structure[76,77] and, concomitantly, of properties.[33] Isotope effects aside, the neutron pair distribution functions (NPDFs) shown in Figure 6 exhibit clear features associated with changes in molecular motion with temperature. By comparison with the reported X-ray pair distribution function (XPDF, which will have a negligible contribution from the weakly-scattering organic molecule) for hydrogenated $FAPbI_3$[56] and the calculated NPDF for the isolated molecule (molecular geometry from DFT, Supporting Information Figure S5), we identify regions with substantial temperature dependence due to atom–atom

correlations between the molecule and the inorganic framework.

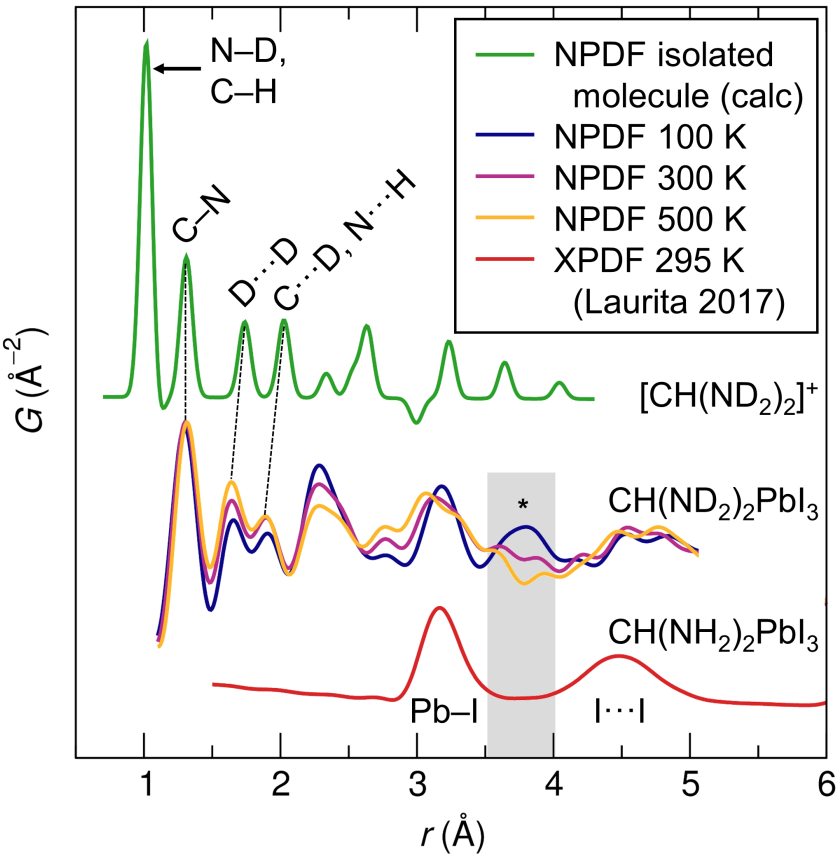

Figure 6: Neutron pair distribution functions (NPDF) for N-deuterated perovskite $FAPbI_3$ from neutron total scattering experiments, with the calculated NPDF for an isolated N-deuterated FA cation (molecular geometry from DFT, Figure S5), and the reported X-ray pair distribution function (XPDF)[56] for comparison. (*) Particularly around ≈3.7 Å, which corresponds to N···I correlations (see supporting information Figure S6, as well as Steiner's crystallographic database analysis of hydrogen bonding),[78] the NPDFs are significantly sharpened on cooling, consistent with a reduced reorientation rate of the molecule.

Of particular note, the PDF is significantly enhanced and sharpened with cooling near ≈3.7 Å, consistent with a slowing of molecular motion. This distance corresponds to the N···I separation for hydrogen bonds between $–N sp^2H_2$ donors and iodine acceptors from ab initio structure relaxations (3.6 Å to 3.7 Å, supporting information) and from the crystallographic database analysis of Steiner (3.66 Å).[78]

This evidence of molecule–cage correlations at distances consistent with hydrogen bonding suggests the importance of the molecule–cage interaction for correctly describing

local structure and lattice dynamics. Indeed, local distortions enhanced by the molecules have recently been implicated in the anomalously large bandgaps of the hybrid perovskites relative to their all-inorganic counterparts,[79] and the hydrogen bonds in $MAPbI_3$ are suggested to play an important role in directing structure evolution more broadly.[34,38,39] It appears likely that standard methods for calculating phonon dispersions may fall short given the sensitivity of lattice stiffness to the particular ordering of molecular orientations (due to hydrogen bonding) and the overlapping timescales for molecular reorientation and phonons.

An overview of the evolution of crystal structure and molecular dynamics for the known phases of $FAPbI_3$ and $MAPbI_3$, as well as the activation barriers for molecular rotations in each, is displayed in Figure 7. This represents a synthesis of the results of this work with the findings of complementary prior reports.[14,16,19,23,29,36,41]

As $FAPbI_3$ is cooled, molecular motion slows and the inorganic octahedra tilt to improve coordination of the *A*-site cation and enhance electrostatic binding, but the molecular geometry appears to be incompatible with the preferred ground state octahedral tilting pattern. This leads to substantially more complex behavior in $FAPbI_3$ than in $MAPbI_3$, with a disordered pseudo-cubic γ-phase with persistent dipole motion,[19] followed by a fragile glassy freezing into a disordered ground state.[14] The activation barriers (above 100 K) for molecular rotation increase monotonically in each successive phase on cooling, reflecting lattice contraction and the increasingly confined local environment of the *A*-site as the degree of octahedral tilting increases. In the case of the disordered, pseudo-cubic γ-phase, the tilt angles increase only locally, but not crystallographically.

In contrast, as $MAPbI_3$ is cooled, the tetragonal β-phase exhibits a tilt pattern ($a^0a^0c^-$) that is unusual for perovskite bromides and iodides,[80] followed by a common orthorhombic tilt pattern ($a^+b^-b^-$) that somewhat easily accommodates the shape and hydrogen bonding tendencies of the MA cation in antiferrodistortive ordering. This last transition is accompanied by the loss of four-fold dipole reorientation, which drastically reduces the di-

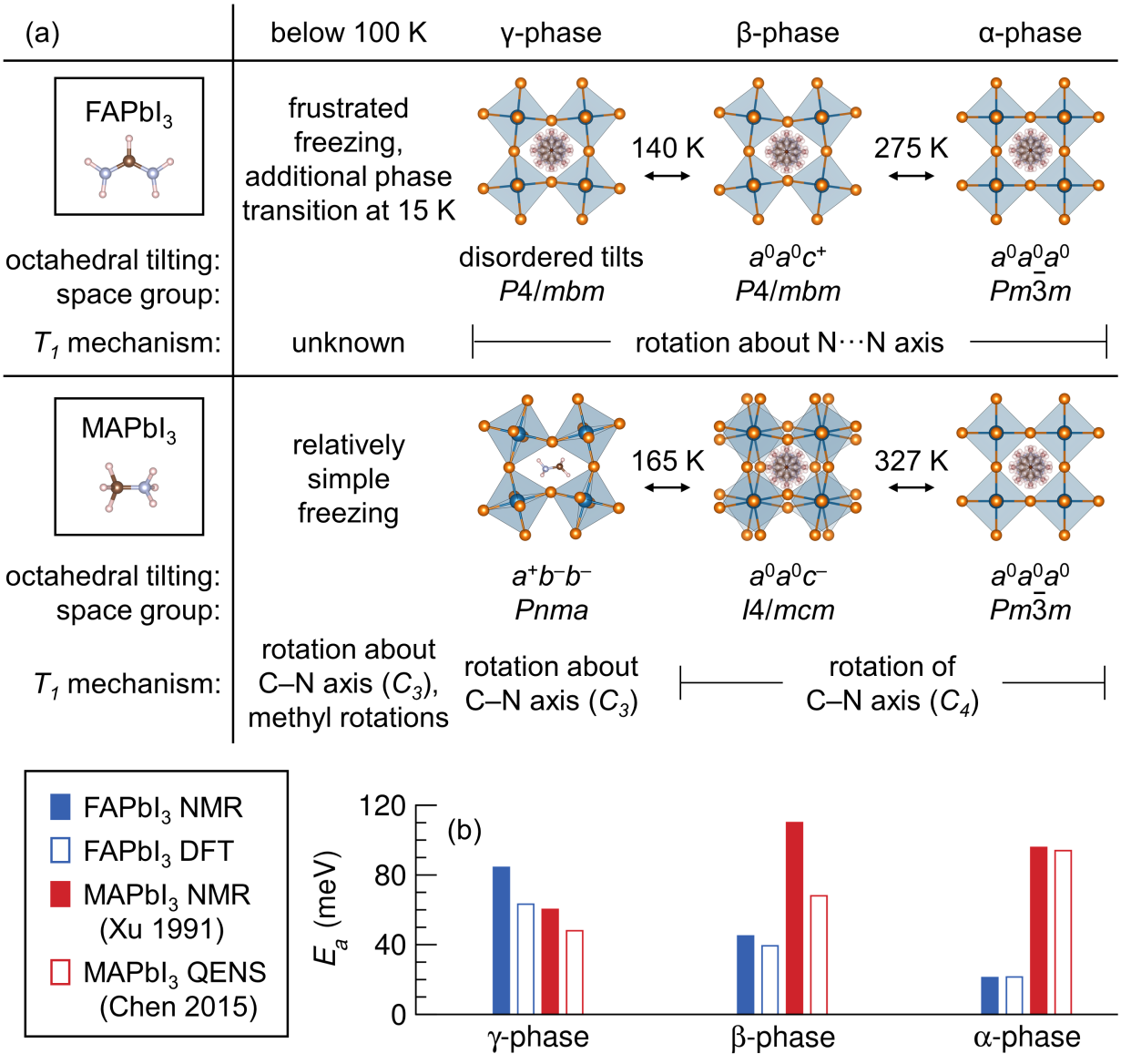

Figure 7: (a) Overview of the temperature evolution of crystal structure and molecular rotations for $FAPbI_3$ and $MAPbI_3$. Crystal structures and phase transition temperatures are taken from Weller and coworkers[41] and Fabini and coworkers,[19] while T_1 mechanisms and low temperature behaviors ($<$100 K) are synthesized from this work and prior reports.[14,16,19,23,29,36] (b) Activation barriers for molecular rotation mechanisms that mediate spin-lattice relaxation for the known perovskite phases of $FAPbI_3$ and $MAPbI_3$. Values for $FAPbI_3$ are from this work, while those for $MAPbI_3$ are drawn from the literature.[23,29]

electric response and leads to a reduced activation barrier for rotation from ^{1}H NMR, since relatively facile three-fold rotations about the C–N axis become the dominant relaxation mechanism. While signatures of glassy freezing exist on cooling this compound below 100 K, they are significantly subtler than for $FAPbI_3$,[14] which comports with the findings presented here.

Conclusion

With $FAPbI_3$ the closest end-member of the highest performing perovskite photovoltaic absorber solid solutions, establishing the dynamics of molecular motion is an important prerequisite for mechanistic explanations of the outstanding optoelectronic properties of these systems. We show via spectroscopy, scattering, calorimetry, and computation that despite differences in the details of the molecule–cage interaction in $FAPbI_3$ and the better-studied $MAPbI_3$, reorientation rates of the molecular dipole axis at room temperature are not significantly different in the two. Both systems coincidentally exhibit reorientation times on the order of 8 ps at ambient temperature, with weaker temperature dependence in $FAPbI_3$. For FA, rotations about an axis parallel to the N···N line are the preferred mode in all phases above ≈50 K. Incompatibility between the geometry of hydrogen bonding propensities of the molecule and octahedral tilting tendencies of the inorganic framework lead to a frustrated molecule–cage interaction. As the system is cooled, this frustration produces an unusual disordered phase with reentrant cubic pseudosymmetry followed by a glassy freezing into a disordered ground state. Hydrogen bonds between amine group hydrogens and the halogens of the surrounding cage underscore the importance of the molecular cation in directing structure evolution and modifying the electron–phonon coupling.

This work provides essential dynamical and structural information for resolving the key outstanding questions in the halide perovskite field: Namely, why are these solution-processed materials so insensitive to inevitable point defects and impurities; why are car-

rier mobilities so modest relative to the expectation from the low effective masses indicated from band theory; and how can strong optical absorption and extremely long carrier lifetimes fortuitously coexist? Because of the couplings between molecular motion and dielectric response, local electric fields, dynamic symmetry-breaking, and electron–phonon scattering, any hypothesis which attempts to explain these (including those of large-polaron transport and of transient Rashba–Dresselhaus effects) must reconcile with this emerging understanding of molecular motions.

Time-resolved spectroscopic[81] and scattering[82] techniques may afford the opportunity to probe these promising semiconductors on time-scales relevant to the structural and electronic perturbations that are proposed to play a role in enhanced carrier lifetimes.[22,48–50,53,56–58,83] We hope that new results such as these may inform a key point of contention: Are the molecular cations simply larger monocations than any (non-radioactive) alkali metal (in a sense, "pseudo-francium") that serves to un-tilt the surrounding inorganic framework and improve orbital overlap, or are they indeed intimately linked to the remarkable functionality of these intriguing materials?

Methods

$HC(NH_2)_2PbI_3$ samples for all experiments except neutron total scattering were prepared as described previously,[19] and $HC(ND_2)_2PbI_3$ samples were prepared following a modification of the previously reported procedure, as described below.[40] PbO and $HC(NH_2)_2Cl$ were purchased from Sigma-Aldrich. 10 M solutions of the $HC(NH_2)_2Cl$ in D_2O were prepared by dissolving 8.05 g of $HC(NH_2)_2Cl$ in 10 mL D_2O and left standing for 24 h prior to use. 4.46 g (20 mmol) of PbO were initially dissolved in 15 ml of concentrated aqueous HI (57% w/w) and the solution temperature was raised and held to boiling (ca. 130° C) to afford a clear yellow solution. Addition of 2 mL of a 10 M solution of $HC(NH_2)_2Cl$ in D_2O resulted immediately in the precipitation of a fine black precipitate. The solution was

stirred for 1 min and filtered hot under vacuum to avoid the exchange of the deuterium atoms with the hydrogen atoms. During filtration the black solid turns to yellow completely converting over a period of 5 to 10 min. The dry yellow solid produced 9 g (71% yield based on Pb) of crystallographically pure material.

Solid state ^{1}H NMR experiments and T_1 relaxation measurements under magic angle spinning (MAS) near ambient temperature were conducted on a 500 MHz (11.7 T) Bruker Avance NMR spectrometer with a Bruker 4 mm H/X/Y triple resonance MAS probe. Powdered samples were packed into a 4 mm zirconia MAS rotor and capped with a Vespel drive cap. For the black perovskite phase, the uncapped, packed rotor was first heated at $\approx$150° C under dynamic vacuum overnight to ensure complete conversion to the black phase and prevent subsequent degradation to the yellow phase, as described previously.[19] ^{1}H chemical shift was referenced to adamantane (1.71 ppm relative to TMS at 0 ppm). Longitudinal relaxation (T_1) experiments utilized the inversion recovery method. All gas flows (for MAS and temperature control) were dry nitrogen to reduce the risk of sample degradation to the yellow δ-phase, which appears to be hastened by moisture. Sample temperature was calibrated with the ^{207}Pb signal of lead nitrate[84] under the same MAS conditions, and the probehead was allowed to equilibrate for one hour at each temperature point before data acquisition.

Static solid state ^{1}H NMR experiments below 200 K were conducted in a 300 MHz (7.05 T) Bruker Avance DSX spectrometer equipped with a homebuilt NMR probe with slight modifications from descriptions in previous publications.[85,86] The powdered sample was packed in a Kel-F (CTFE) sample cup with inner and outer diameters of 5.3 mm and 7 mm, respectively, and height of 8 mm. After packing the sample cup, the sample cup was covered using a Kel-F cap, and immediately placed into the NMR probe for cryogenic cooling. The NMR probe is placed within a STVP-200-NMR cryostat (Janis Research Company) where a continuous flow of vaporized liquid helium is used to cool the entire NMR probe and sample. Temperature control is achieved with a combination of continuous cold

helium gas flow and a resistive heater. The temperature is monitored with a Cernox sensor mounted on the cryostat at the sample position, while the heater output of the resistive heater was controlled with a PID algorithm in LabView that controls the voltage level of the resistive heater in relation to the desired temperature setpoint. The temperature is maintained at an accuracy level of +/–50 mK or better, depending on the temperature range. The probehead was allowed to equilibrate for 15 to 30 minutes at each setpoint before data acquisition, depending on the temperature step. Longitudinal relaxation experiments utilized the saturation recovery method. A small impurity of the yellow δ-phase was detected due to brief sample preparation in air, which was reflected in a second T_1 feature. To account for this, a constrained fitting routine was written in `python` utilizing the least-squares minimization package `lmfit`[87] which constrained the ratio of the black and yellow phase fractions (a fitting parameter) across all experiments for each non-consecutive day of data acquisition, while other parameters (relaxation times, amplitudes) were allowed to vary independently. The data were well modeled by this approach, and T_1 of the black phase was evident as the dominant contribution. The phase fraction of the yellow impurity phase ranged from 10% to 20% across the various non-consecutive days of the experiment. Cross-checking against the measured T_1 times for pure black $FAPbI_3$ (Figure 1) between 220 K and 340 K and pure yellow $FAPbI_3$ at 300 K (unpublished) ensured there was no amiguity in assigning the two T_1 features to the pertinent polymorphs.

Dielectric spectroscopy was performed as described previously.[19] Heat capacity measurements across phase transitions were carried out via the pulsed dual-slope analysis method in a Quantum Design PPMS cryostat under high vacuum (9×10^{-6} Torr). Polycrystalline samples were ground, mixed with powdered iron (51.52% by mass, to enhance thermal conductivity), and cold-pressed to 1 t in a 3 mm $\times$ 9 mm die. The pellet was shattered, and a flat shard (5.00 mg) was measured. The background was subtracted by separately measuring a similarly prepared sample of the iron diluent (8.10 mg), and the heat capacity of the composite sample was assumed to be a simple linear combination of

the two. For the rotational freezing region ($\approx$ 50 K), a T-rise of 30 K from 30 K was employed, and measured time constants were $\tau_1 \approx 25$ s, $\tau_2 = 0$ s (strong thermal coupling). For the β–γ transition ($\approx$ 140 K), a temperature rise of 50 K from 110 K was employed, and measured time constants were $\tau_1 \approx 54$ s, $\tau_2 = 0$ s (strong thermal coupling). All measurements were repeated three times.

Neutron total scattering experiments were performed on an N-deuterated sample using the NOMAD instrument (BL-1B)[88] at the Spallation Neutron Source at Oak Ridge National Laboratory. The as-prepared dried powders were transferred into a mortar and pestle and thoroughly ground to a fine powder. The sample was packed into a 6 mm diameter vanadium canister and sealed tightly under N_2 atmosphere. Measurements were performed in an approximately 1.5 cm cross-section neutron beam, and the detectors were calibrated with scattering data from a diamond powder standard prior to measurements. The sample temperature was first raised to 500 K to ensure complete conversion to the black perovskite phase, and subsequently cooled to 300 K and then 100 K. Approximate data collection times were 20 mins at 500 K and 2 hr each at 300 K and 100 K. Data were normalized against scattering data collected for a vanadium rod, container background was subtracted, and the merged total scattering structure function was produced using the IDL codes developed for the NOMAD instrument.[88] Significant incoherent scattering necessitated hydrogen correction of the structure functions, following the procedure of Page and coworkers,[89] with the parameters $L = 0$, $u^2 = 0.05$ Å^2 (the salient features of the PDFs shown in Figure 6 were found to be robust to variation of these parameters). Fourier transforms of the corrected structure factors were performed with Q_{min} = 1.0 Å^{-1}, Q_{max} = 21.88 Å^{-1}. Hydrogen corrections[89] and the generation of PDFs were performed using custom `python` code. Simulated neutron PDFs for analysis were generated using the PDFgui software suite.[90]

Fourier difference maps were generated from high-resolution synchrotron X-ray powder diffraction experiments at beamline 11-BM of the Advanced Photon Source at Argonne Na-

tional Laboratory that have been described previously.[19] The *A*-site molecule was removed from the crystal structure models from Rietveld refinement,[19] and the residual charge density was calculated using the program GSAS[91] with the interface EXPGUI.[92] Results were visualized with VESTA[93] and custom `python` code.

Ab initio calculations of the molecule geometry and energy surfaces for molecular rotation were performed with the Vienna Ab initio Simulation Package (VASP),[94–97] which implements the Kohn–Sham formulation of density functional theory (DFT) using a plane wave basis set and the projector augmented wave formalism.[98,99] The generalized gradient approximation was employed using the revised exchange and correlation functional for solids of Perdew, Burke, and Ernzerhof (GGA–PBEsol).[100] For Pb, d electrons were included in the valence. The plane wave basis set cutoff energy (800 eV) and k-point mesh density (α-phase: $6 \times 6 \times 6$; β-,γ-phases: $4 \times 4 \times 6$, both Γ-centered Monkhorst–Pack sampling[101] for molecular rotations) were chosen based on convergence of the total energy.

To map the energy surfaces for molecular rotation, the structure of the isolated molecular cation was first relaxed in a $(16\,\text{Å})^3$ cube (to avoid interaction with periodic images) with a homogeneous neutralizing background jellium. Rigid rotations and translations of the molecule were then generated using Euler angle-based rotations in a custom `python` program, and the total energies evaluated with static DFT calculations. Lattice parameters and inorganic atom positions were fixed to those observed in experiment,[19] and deformations of the inorganic framework were not considered. The nominal orientations of the molecule are depicted in Figure 4, with the dipole axes (C–H) oriented ferroically from cell to cell (all parallel to c). For rotations about each principle direction of a coordinate system fixed to the molecule, a 2-D translation-rotation study was performed, and the minimum energy path for rotation was extracted.

Supporting Information

^{1}H MAS NMR spectra of α-$FAPbI_3$ (black) and δ-$FAPbI_3$ (yellow), calorimetry across the rotational freezing transition (≈50 K) and across the β–γ transition (≈140 K), Fourier difference maps from X-ray diffraction for analysis of preferred molecular orientations, molecular geometries from ab initio calculations, analysis of hydrogen bonding geometries.

Author Information

Corresponding Author

seshadri@mrl.ucsb.edu

The authors declare no competing financial interest.

Acknowledgement

We thank Catherine Oertel (Oberlin College) for her useful suggestions. This work was supported by the U.S. Department of Energy, Office of Science, Basic Energy Sciences under award number DE-SC-0012541. DHF thanks the National Science Foundation Graduate Research Fellowship Program for support under Grant DGE 1144085. The authors acknowledge a financial gift from JEOL that supported the postdoctoral appointment of TAS and aspects of the NMR instrument development. The contributions by KP and DO were supported through the U.S. Department of Energy, Office of Science, Office of Basic Energy Sciences, Early Career Research Program award KC040602, under contract number DE-AC05-00OR22725. A portion of this research used resources at the Spallation Neutron Source, a DOE Office of Science User Facility operated by the Oak Ridge National Laboratory, and resources of the Advanced Photon Source, a DOE Office of Science User Facility operated for the DOE Office of Science by Argonne National Laboratory under Contract No. DE-AC02-06CH11357. Extensive use of the Shared Experimental Facilities of the Ma-

terials Research Science and Engineering Center at UCSB (MRSEC NSF DMR 1720256) is gratefully acknowledged. The UCSB MRSEC is a member of the NSF-supported Materials Research Facilities Network (www.mrfn.org). We additionally acknowledge support from the Center for Scientific Computing from the CNSI, MRL: an NSF MRSEC (DMR-1720256) and NSF CNS-0960316.

References

(1) Lotsch, B. V. *Angew. Chem. Int. Ed.* **2014**, *53*, 635–637.

(2) Stoumpos, C. C.; Kanatzidis, M. G. *Acc. Chem. Res.* **2015**, *48*, 2791–2802.

(3) Saparov, B.; Mitzi, D. B. *Chem. Rev.* **2016**, *116*, 4558–4596.

(4) Fabini, D. H.; Labram, J. G.; Lehner, A. J.; Bechtel, J. S.; Evans, H. A.; Van der Ven, A.; Wudl, F.; Chabinyc, M. L.; Seshadri, R. *Inorg. Chem.* **2016**, *56*, 11–25.

(5) Sherwood, J. N., Ed. *The plastically crystalline state: Orientationally disordered crystals*; Wiley: Chichester, U.K., 1979.

(6) Purcell, E. *Physica* **1951**, *17*, 282–302.

(7) Woessner, D. E.; Jr., B. S. S. *J. Chem. Phys.* **1967**, *47*, 378–381.

(8) Blinc, R.; Seliger, J.; Dolinšek, J.; Arčon, D. *Phys. Rev. B* **1994**, *49*, 4993–5002.

(9) Kojima, A.; Teshima, K.; Shirai, Y.; Miyasaka, T. *J. Am. Chem. Soc.* **2009**, *131*, 6050–6051.

(10) Lee, M. M.; Teuscher, J.; Miyasaka, T.; Murakami, T. N.; Snaith, H. J. *Science* **2012**, *338*, 643–647.

(11) Saliba, M.; Matsui, T.; Seo, J.-Y.; Domanski, K.; Correa-Baena, J.-P.; Nazeeruddin, M. K.; Zakeeruddin, S. M.; Tress, W.; Abate, A.; Hagfeldt, A.; Grätzel, M. *Energy Environ. Sci.* **2016**, *9*, 1989–1997.

(12) Weber, D. *Z. Naturforsch. B Chem. Sci.* **1978**, *33*, 1443–1445.

(13) Onoda-Yamamuro, N.; Matsuo, T.; Suga, H. *J. Phys. Chem. Solids* **1990**, *51*, 1383–1395.

(14) Fabini, D. H.; Hogan, T.; Evans, H. A.; Stoumpos, C. C.; Kanatzidis, M. G.; Seshadri, R. *J. Phys. Chem. Lett.* **2016**, *7*, 376–381.

(15) Poglitsch, A.; Weber, D. *J. Chem. Phys.* **1987**, *87*, 6373–6378.

(16) Bakulin, A. A.; Selig, O.; Bakker, H. J.; Rezus, Y. L.; Mller, C.; Glaser, T.; Lovrincic, R.; Sun, Z.; Chen, Z.; Walsh, A.; Frost, J. M.; Jansen, T. L. C. *J. Phys. Chem. Lett.* **2015**, *6*, 3663–3669.

(17) Onoda-Yamamuro, N.; Matsuo, T.; Suga, H. *J. Phys. Chem. Solids* **1992**, *53*, 935–939.

(18) Maeda, M.; Hattori, M.; Hotta, A.; Suzuki, I. *J. Phys. Soc. Jpn.* **1997**, *66*, 1508–1511.

(19) Fabini, D. H.; Stoumpos, C. C.; Laurita, G.; Kaltzoglou, A.; Kontos, A. G.; Falaras, P.; Kanatzidis, M. G.; Seshadri, R. *Angew. Chem. Int. Ed.* **2016**, *55*, 15392–15396.

(20) Anusca, I.; Balinas, S.; Gemeiner, P.; Svirskas, .; Sanlialp, M.; Lackner, G.; Fettkenhauer, C.; Belovickis, J.; Samulionis, V.; Ivanov, M.; Dkhil, B.; Banys, J.; Shvartsman, V. V.; Lupascu, D. C. *Adv. Energy Mater.* **2017**, 1700600.

(21) Guo, Y.; Yaffe, O.; Paley, D. W.; Beecher, A. N.; Hull, T. D.; Szpak, G.; Owen, J. S.; Brus, L. E.; Pimenta, M. A. *Phys. Rev. Materials* **2017**, *1*, 042401(R).

(22) Swainson, I. P.; Stock, C.; Parker, S. F.; Van Eijck, L.; Russina, M.; Taylor, J. W. *Phys. Rev. B* **2015**, *92*, 100303.

(23) Chen, T.; Foley, B. J.; Ipek, B.; Tyagi, M.; Copley, J. R. D.; Brown, C. M.; Choi, J. J.; Lee, S.-H. *Phys. Chem. Chem. Phys.* **2015**, *17*, 31278–31286.

(24) Leguy, A. M. A.; Frost, J. M.; McMahon, A. P.; Sakai, V. G.; Kockelmann, W.; Law, C.; Li, X.; Foglia, F.; Walsh, A.; O'Regan, B. C.; Nelson, J.; Cabral, J. T.; Barnes, P. R. F. *Nat. Commun.* **2015**, *6*, 7124.

(25) Drużbicki, K.; Pinna, R. S.; Rudić, S.; Jura, M.; Gorini, G.; Fernandez-Alonso, F. *J. Phys. Chem. Lett.* **2016**, *7*, 4701–4709.

(26) Li, B.; Kawakita, Y.; Liu, Y.; Wang, M.; Matsuura, M.; Shibata, K.; Ohira-Kawamura, S.; Yamada, T.; Lin, S.; Nakajima, K.; Liu, S. F. *Nat. Commun.* **2017**, *8*, 16086.

(27) Wasylishen, R. E.; Knop, O.; Macdonald, J. B. *Solid State Commun.* **1985**, *56*, 581–582.

(28) Knop, O.; Wasylishen, R. E.; White, M. A.; Cameron, T. S.; Oort, M. J. M. V. *Can. J. Chem.* **1990**, *68*, 412–422.

(29) Xu, Q.; Eguchi, T.; Nakayama, H.; Nakamura, N.; Kishita, M. *Z. Naturforsch. A* **1991**, *46*, 240–246.

(30) Rosales, B. A.; Men, L.; Cady, S. D.; Hanrahan, M. P.; Rossini, A. J.; Vela, J. *Chem. Mater.* **2016**, *28*, 6848–6859.

(31) Roiland, C.; Trippe-Allard, G.; Jemli, K.; Alonso, B.; Ameline, J.-C.; Gautier, R.; Bataille, T.; Le Polles, L.; Deleporte, E.; Even, J.; Katan, C. *Phys. Chem. Chem. Phys.* **2016**, *18*, 27133–27142.

(32) Franssen, W. M. J.; van Es, S. G. D.; Derviolu, R.; de Wijs, G. A.; Kentgens, A. P. M. *J. Phys. Chem. Lett.* **2017**, *8*, 61–66.

(33) Gong, J.; Yang, M.; Ma, X.; Schaller, R. D.; Liu, G.; Kong, L.; Yang, Y.; Beard, M. C.; Lesslie, M.; Dai, Y.; Huang, B.; Zhu, K.; Xu, T. *J. Phys. Chem. Lett.* **2016**, *7*, 2879–2887.

(34) Lee, J.-H.; Bristowe, N. C.; Bristowe, P. D.; Cheetham, A. K. *Chem. Commun.* **2015**, *51*, 6434–6437.

(35) Even, J.; Carignano, M.; Katan, C. *Nanoscale* **2016**, *8*, 6222–6236.

(36) Carignano, M. A.; Saeed, Y.; Aravindh, S. A.; Roqan, I. S.; Even, J.; Katan, C. *Phys. Chem. Chem. Phys.* **2016**, *18*, 27109–27118.

(37) Bechtel, J. S.; Seshadri, R.; Van der Ven, A. *J. Phys. Chem. C* **2016**, *120*, 12403–12410.

(38) Lee, J.-H.; Bristowe, N. C.; Lee, J. H.; Lee, S.-H.; Bristowe, P. D.; Cheetham, A. K.; Jang, H. M. *Chem. Mater.* **2016**, *28*, 4259–4266.

(39) Lee, J. H.; Lee, J.-H.; Kong, E.-H.; Jang, H. M. *Sci. Rep.* **2016**, *6*, 21687.

(40) Stoumpos, C. C.; Malliakas, C. D.; Kanatzidis, M. G. *Inorg. Chem.* **2013**, *52*, 9019–9038.

(41) Weller, M. T.; Weber, O. J.; Henry, P. F.; Di Pumpo, A. M.; Hansen, T. C. *Chem. Commun.* **2015**, *51*, 4180–4183.

(42) Weller, M. T.; Weber, O. J.; Frost, J. M.; Walsh, A. *J. Phys. Chem. Lett.* **2015**, *6*, 3209–3212.

(43) Weber, O. J.; Charles, B.; Weller, M. T. *J. Mater. Chem. A* **2016**, *4*, 15375–15382.

(44) Chen, T.; Foley, B. J.; Park, C.; Brown, C. M.; Harriger, L. W.; Lee, J.; Ruff, J.; Yoon, M.; Choi, J. J.; Lee, S.-H. *Sci. Adv.* **2016**, *2*, e1601650.

(45) Sun, S.; Deng, Z.; Wu, Y.; Wei, F.; Halis Isikgor, F.; Brivio, F.; Gaultois, M. W.; Ouyang, J.; Bristowe, P. D.; Cheetham, A. K.; Kieslich, G. *Chem. Commun.* **2017**, *53*, 7537–7540.

(46) Whitfield, P.; Herron, N.; Guise, W.; Page, K.; Cheng, Y.; Milas, I.; Crawford, M. *Sci. Rep.* **2016**, *6*, 35685.

(47) Frost, J. M.; Butler, K. T.; Brivio, F.; Hendon, C. H.; Van Schilfgaarde, M.; Walsh, A. *Nano Lett.* **2014**, *14*, 2584–2590.

(48) Zhu, X.-Y.; Podzorov, V. *J. Phys. Chem. Lett.* **2015**, *6*, 4758–4761.

(49) Zhu, H.; Miyata, K.; Fu, Y.; Wang, J.; Joshi, P. P.; Niesner, D.; Williams, K. W.; Jin, S.; Zhu, X.-Y. *Science* **2016**, *353*, 1409–1413.

(50) Kim, M.; Im, J.; Freeman, A. J.; Ihm, J.; Jin, H. *Proc. Natl. Acad. Sci. USA* **2014**, *111*, 6900–6904.

(51) Brgoch, J.; Lehner, A. J.; Chabinyc, M. L.; Seshadri, R. *J. Phys. Chem. C* **2014**, *18*, 27721–27727.

(52) Stoumpos, C. C.; Frazer, L.; Clark, D. J.; Kim, Y. S.; Rhim, S. H.; Freeman, A. J.; Ketterson, J. B.; Jang, J. I.; Kanatzidis, M. G. *J. Am. Chem. Soc.* **2015**, *137*, 6804–6819.

(53) Fabini, D. H.; Laurita, G.; Bechtel, J. S.; Stoumpos, C. C.; Evans, H. A.; Kontos, A. G.; Raptis, Y. S.; Falaras, P.; Van der Ven, A.; Kanatzidis, M. G.; Seshadri, R. *J. Am. Chem. Soc.* **2016**, *138*, 11820–11832.

(54) Zhu, H.; Trinh, M. T.; Wang, J.; Fu, Y.; Joshi, P. P.; Miyata, K.; Jin, S.; Zhu, X.-Y. *Adv. Mater.* **2016**, *29*, 1603072.

(55) Beecher, A. N.; Semonin, O. E.; Skelton, J. M.; Frost, J. M.; Terban, M. W.; Zhai, H.; Alatas, A.; Owen, J. S.; Walsh, A.; Billinge, S. J. L. *ACS Energy Lett.* **2016**, *1*, 880–887.

(56) Laurita, G.; Fabini, D. H.; Stoumpos, C. C.; Kanatzidis, M. G.; Seshadri, R. *Chem. Sci.* **2017**, *8*, 5628–5635.

(57) Yaffe, O.; Guo, Y.; Tan, L. Z.; Egger, D. A.; Hull, T.; Stoumpos, C. C.; Zheng, F.; Heinz, T. F.; Kronik, L.; Kanatzidis, M. G.; Owen, J. S.; Rappe, A. M.; Pimenta, M. A.; Brus, L. E. *Phys. Rev. Lett.* **2017**, *118*, 136001.

(58) Marronnier, A.; Lee, H.; Geffroy, B.; Even, J.; Bonnassieux, Y.; Roma, G. *J. Phys. Chem. Lett.* **2017**, *8*, 2659–2665.

(59) Smith, M. D.; Jaffe, A.; Dohner, E. R.; Lindenberg, A. M.; Karunadasa, H. I. *Chem. Sci.* **2017**, *8*, 4497–4504.

(60) Kulbak, M.; Cahen, D.; Hodes, G. *J. Phys. Chem. Lett.* **2015**, *6*, 2452–2456.

(61) Eperon, G. E.; Paternò, G. M.; Sutton, R. J.; Zampetti, A.; Haghighirad, A. A.; Cacialli, F.; Snaith, H. J. *J. Mater. Chem. A* **2015**, *3*, 19688–19695.

(62) Gupta, S.; Bendikov, T.; Hodes, G.; Cahen, D. *ACS Energy Lett.* **2016**, *1*, 1028–1033.

(63) Beal, R. E.; Slotcavage, D. J.; Leijtens, T.; Bowring, A. R.; Belisle, R. A.; Nguyen, W. H.; Burkhard, G.; Hoke, E. T.; McGehee, M. D. *J. Phys. Chem. Lett.* **2016**, *7*, 746–751.

(64) Hutter, E. M.; Sutton, R. J.; Chandrashekar, S.; Abdi-Jalebi, M.; Stranks, S. D.; Snaith, H. J.; Savenije, T. J. *ACS Energy Lett.* **2017**, *2*, 1901–1908.

(65) Owens, F. J., Poole, C. P., Jr., Farach, H. A., Eds. *Magnetic resonance of phase transitions*; Academic Press, Inc.: New York, 1979.

(66) Xu, Q.; Eguchi, T.; Nakayama, H. *Bull. Chem. Soc. Jpn.* **1992**, *65*, 2264–2266.

(67) Senthil Kumaran, S.; Ramesh, K.; Ramakrishna, J. *Phase Transit.* **2002**, *75*, 597–605.

(68) Besara, T.; Jain, P.; Dalal, N. S.; Kuhns, P. L.; Reyes, A. P.; Kroto, H. W.; Cheetham, A. K. *Proc. Natl. Acad. Sci. U.S.A.* **2011**, *108*, 6828–6832.

(69) Kieslich, G.; Forse, A. C.; Sun, S.; Butler, K. T.; Kumagai, S.; Wu, Y.; Warren, M. R.; Walsh, A.; Grey, C. P.; Cheetham, A. K. *Chem. Mater.* **2016**, *28*, 312–317.

(70) Abhyankar, N.; Kweon, J. J.; Orio, M.; Bertaina, S.; Lee, M.; Choi, E. S.; Fu, R.; Dalal, N. S. *J. Phys. Chem. C* **2017**, *121*, 6314–6322.

(71) Angell, C. A. *Science* **1995**, *267*, 1924–1935.

(72) Bloembergen, N.; Purcell, E. M.; Pound, R. V. *Phys. Rev.* **1948**, *73*, 679–712.

(73) Kubicki, D.; Prochowicz, D.; Hofstetter, A.; Péchy, P.; Zakeeruddin, S. M.; Grätzel, M.; Emsley, L. *J. Am. Chem. Soc.* **2017**, *139*, 10055–10061.

(74) Lin, Q.; Armin, A.; Nagiri, R. C. R.; Burn, P. L.; Meredith, P. *Nat. Photon.* **2015**, *9*, 106–112.

(75) Rao, C. N. R. *J. Chem. Soc., Faraday Trans. 1* **1975**, *71*, 980–983.

(76) Yamada, K.; Mikawa, K.; Okuda, T.; Knight, K. S. *Dalton Trans.* **2002**, 2112–2118.

(77) Swainson, I.; Chi, L.; Her, J.-H.; Cranswick, L.; Stephens, P.; Winkler, B.; Wilson, D. J.; Milman, V. *Acta Crystallogr. Sect. B* **2010**, *66*, 422–429.

(78) Steiner, T. *Acta Crystallogr. Sect. B* **1998**, *54*, 456–463.

(79) Linaburg, M. R.; McClure, E. T.; Majher, J. D.; Woodward, P. M. *Chem. Mater.* **2017**, *29*, 3507–3514.

(80) Young, J.; Rondinelli, J. M. *J. Phys. Chem. Lett.* **2016**, *7*, 918–922.

(81) Sherwin, M. *Nature* **2002**, *420*, 131–133.

(82) Lindenberg, A. M.; Johnson, S. L.; Reis, D. A. *Annu. Rev. Mater. Res.* **2017**, *47*, 425–449.

(83) Zheng, F.; Tan, L. Z.; Liu, S.; Rappe, A. M. *Nano Lett.* **2015**, *15*, 7794–7800.

(84) Bielecki, A.; Burum, D. P. *J. Magn. Reson., Ser A* **1995**, *116*, 215 – 220.

(85) Siaw, T. A.; Walker, S. A.; Armstrong, B. D.; Han, S.-I. *J. Magn. Reson.* **2012**, *221*, 5–10.

(86) Siaw, T. A.; Leavesley, A.; Lund, A.; Kaminker, I.; Han, S. *J. Magn. Reson.* **2016**, *264*, 131–153.

(87) Newville, M.; Stensitzki, T.; Allen, D. B.; Ingargiola, A. LMFIT: Non-Linear Least-Square Minimization and Curve-Fitting for Python. 2014; DOI:10.5281/zenodo.11813.

(88) Neuefeind, J.; Feygenson, M.; Carruth, J.; Hoffmann, R.; Chipley, K. K. *Nucl. Instr. Meth. Phys. Res. B* **2012**, *287*, 68–75.

(89) Page, K.; White, C. E.; Estell, E. G.; Neder, R. B.; Llobet, A.; Proffen, T. *J. Appl. Crystallogr.* **2011**, *44*, 532–539.

(90) Farrow, C.; Juhas, P.; Liu, J.; Bryndin, D.; Božin, E.; Bloch, J.; Proffen, T.; Billinge, S. *J. Phys. Condens. Matter* **2007**, *19*, 335219.

(91) Larson, A. C.; Von Dreele, R. B. *Los Alamos Natl. Lab. Rep. LAUR* **2000**, 86–748.

(92) Toby, B. H. *J. Appl. Crystallogr.* **2001**, *34*, 210–213.

(93) Momma, K.; Izumi, F. *J. Appl. Crystallogr.* **2011**, *44*, 1272–1276.

(94) Kresse, G.; Hafner, J. *Phys. Rev. B* **1993**, *47*, 558–561.

(95) Kresse, G.; Hafner, J. *Phys. Rev. B* **1994**, *49*, 14251–14269.

(96) Kresse, G.; Furthmüller, J. *Phys. Rev. B* **1996**, *54*, 11169–11186.

(97) Kresse, G.; Furthmller, J. *Computat. Mater. Sci.* **1996**, *6*, 15–50.

(98) Blöchl, P. E. *Phys. Rev. B* **1994**, *50*, 17953–17979.

(99) Kresse, G.; Joubert, D. *Phys. Rev. B* **1999**, *59*, 1758–1775.

(100) Perdew, J. P.; Ruzsinszky, A.; Csonka, G. I.; Vydrov, O. A.; Scuseria, G. E.; Constantin, L. A.; Zhou, X.; Burke, K. *Phys. Rev. Lett.* **2008**, *100*, 136406.

(101) Monkhorst, H. J.; Pack, J. D. *Phys. Rev. B* **1976**, *13*, 5188–5192.

Graphical TOC Entry

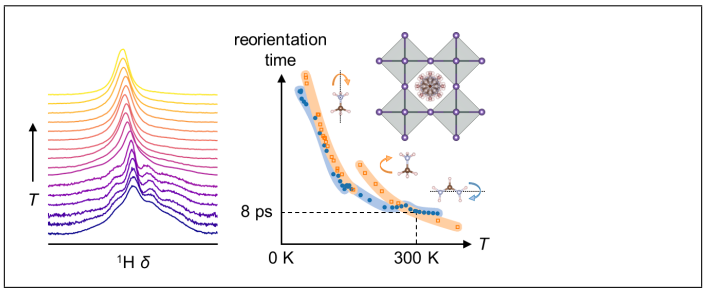

>>> Supporting Information <<<

Universal Dynamics of Molecular Reorientation in Hybrid Lead Iodide Perovskites

Douglas H. Fabini,[†] Ting Ann Siaw,[‡ª] Constantinos C. Stoumpos,[¶] Geneva Laurita,[§] Daniel Olds,[‖] Katharine Page,[‖] Jerry G. Hu,[†] Mercouri G. Kanatzidis,[¶] Songi Han,[‡,⊥] and Ram Seshadri[*,†,‡]

†*Materials Department and Materials Research Laboratory, University of California, Santa Barbara, California 93106, United States*

‡*Department of Chemistry and Biochemistry, University of California, Santa Barbara, California 93106, United States*

¶*Department of Chemistry and Argonne-Northwestern Solar Energy Research Center, Northwestern University, Evanston, Illinois 60208, United States*

§*Department of Chemistry and Biochemistry, Bates College, Lewiston, Maine 04240, United States*

‖*Neutron Scattering Division, Oak Ridge National Laboratory, Oak Ridge, Tennessee 37831, United States*

⊥*Department of Chemical Engineering, University of California, Santa Barbara, California 93106, United States*

E-mail: seshadri@mrl.ucsb.edu

[ª]Current institution: JEOL USA Inc., Peabody, MA 01960, United States

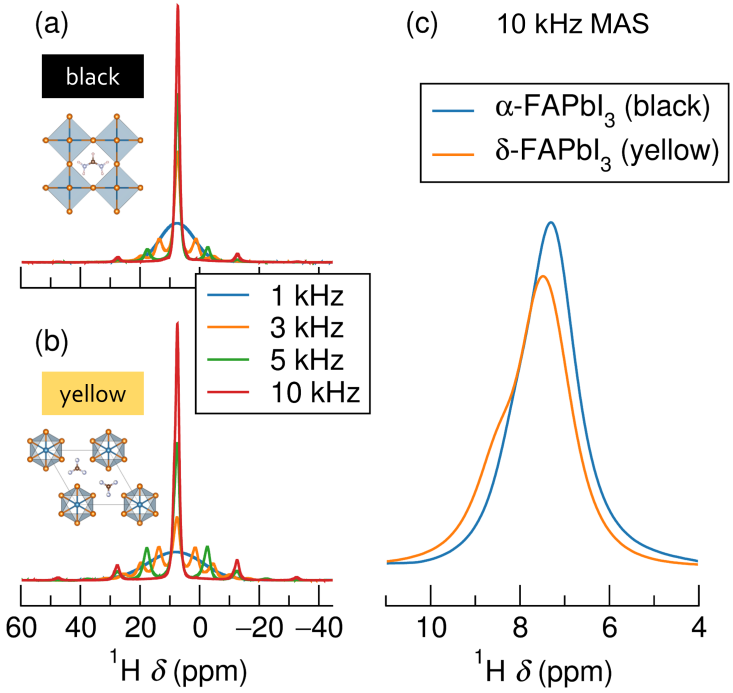

Figure S1: Solid state ^{1}H nuclear magnetic resonance spectra for (a) black α-FAPbI$_3$ and (b) yellow δ-FAPbI$_3$ for various magic-angle spinning (MAS) speeds, at ambient temperature. (c) Detail of the central peak for both phases at 10 kHz MAS. The broader signal and more intense spinning sidebands for the δ-phase are consistent with the anisotropic site symmetry for the disordered molecule in this phase,[1] versus the O_h site symmetry in the α-phase.[2–4]

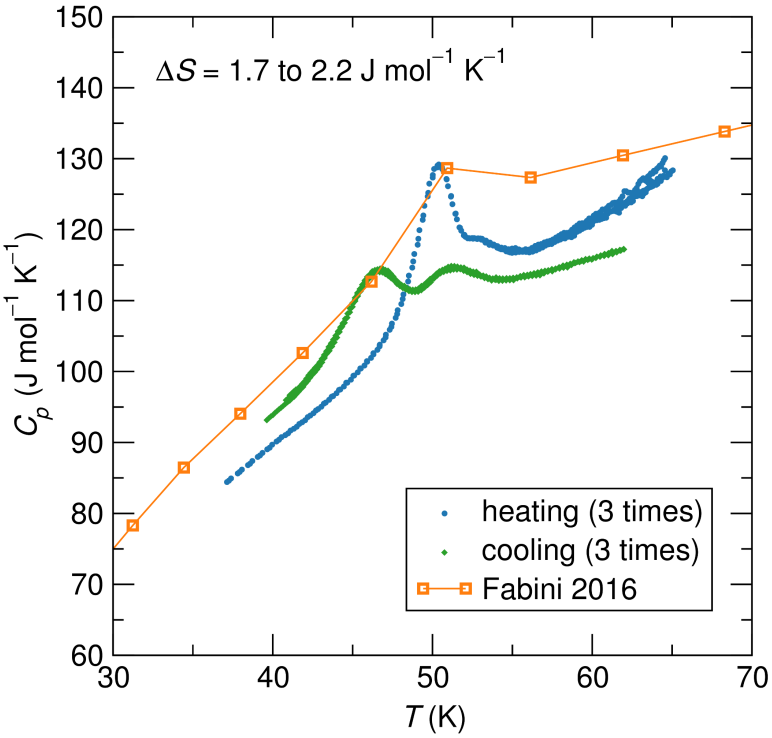

Figure S2: Detail of the heat capacity of $FAPbI_3$ around 50 K based on slope analysis of long heating pulses (values based on short heating pulses from a prior report included for comparison).[5] At least two distinct features are evident, though the total transition entropy ($\sim$2 J mol^{-1} K^{-1}) associated with the excess heat capacity is significantly less than that associated with even a 2-fold order–disorder transition (5.8 J mol^{-1} K^{-1}) The frequency dispersion of the dielectric response[5] in this regime suggests a glassy slowing of molecular motion, rather than a true structural phase transition. The apparent temperature hysteresis may then be due to low thermal conductivity.

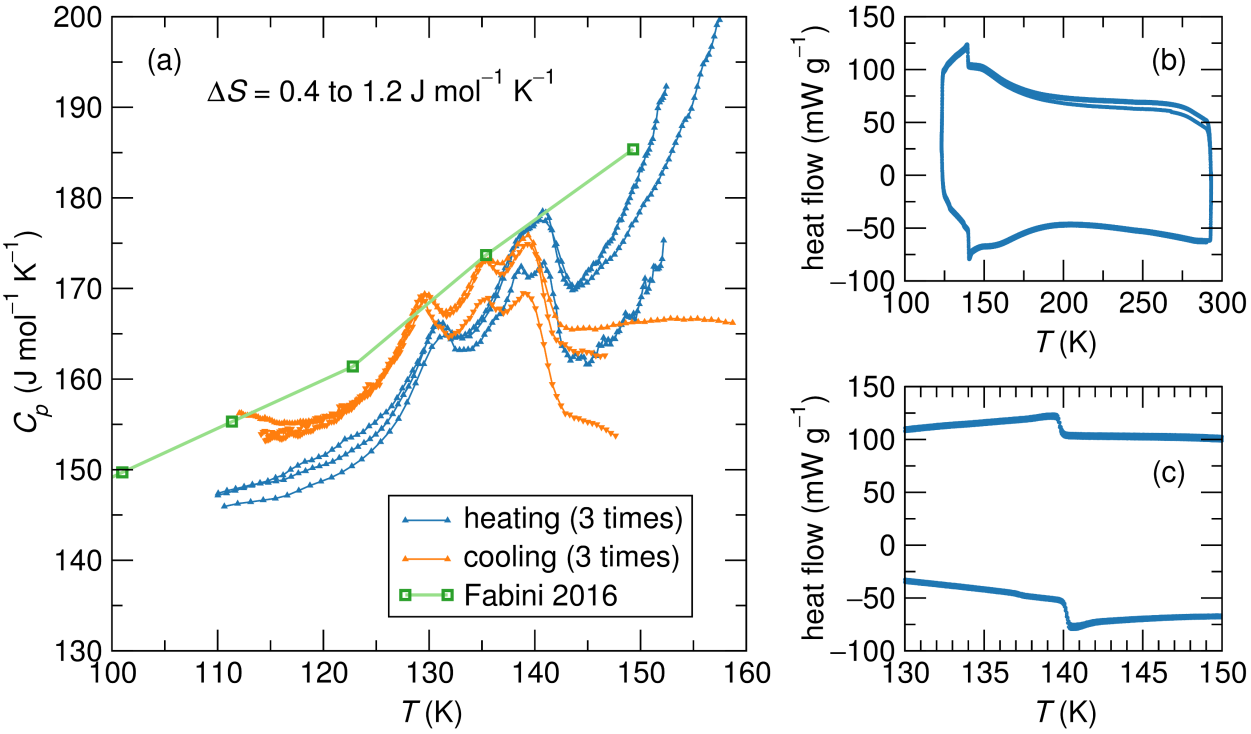

Figure S3: (a) Detail of the heat capacity of $FAPbI_3$ around the β–γ transition based on slope analysis of long heating pulses (values based on short heating pulses from a prior report included for comparison).[5] Despite challenges with low thermal conductivity and high heat capacity in this regime, this reentrant phase transition[3] is revealed to be a complex cascade of multiple events. The total transition entropy ($<1.2\,\mathrm{J\,mol^{-1}\,K^{-1}}$) corresponding to the excess heat capacity is significantly less than that associated with even a 2-fold order–disorder transition ($5.8\,\mathrm{J\,mol^{-1}\,K^{-1}}$). (b,c) Previously reported differential scanning calorimetry[5] does not resolve the multi-step process evident in (a), and the apparent lack of temperature hysteresis in the transition temperature suggests this transition may indeed be continuous rather than first-order.

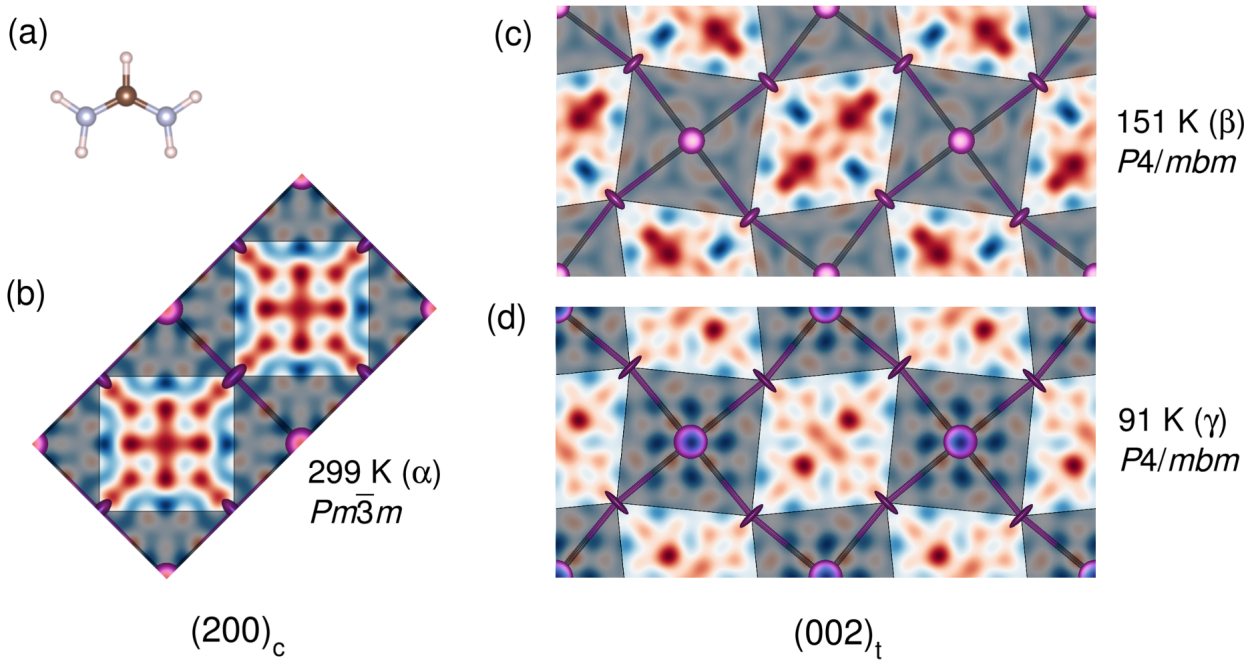

Figure S4: (a) Relaxed geometry of the formadinium ($[CH(NH_2)_2]^+$) cation from DFT calculations. (b-d) Fourier difference maps of the residual electron density associated with the molecular cation in the α-, β-, and γ-phases of $FAPbI_3$, from synchrotron X-ray powder diffraction. This charge density, though only representing $\sim$9% of the electrons, suggests a preference for the $\phi_1 = 90°$ orientation in the tetragonal phases. Though our DFT calculations (Figure 4) find that the absolute energy of this configuration is slightly higher than that of the $\phi_1 = 0°$ orientation, they suggest an entropic stabilization of this orientation (at least above the molecular freezing near 50 K) due to significantly reduced barriers for both ϕ_2 and ϕ_3 molecular rotations. In the cubic phase, the positive residual electron density near the iodides reflects the inadequacy of the Debye-Waller formulation of thermal motion for these highly anharmonic systems.

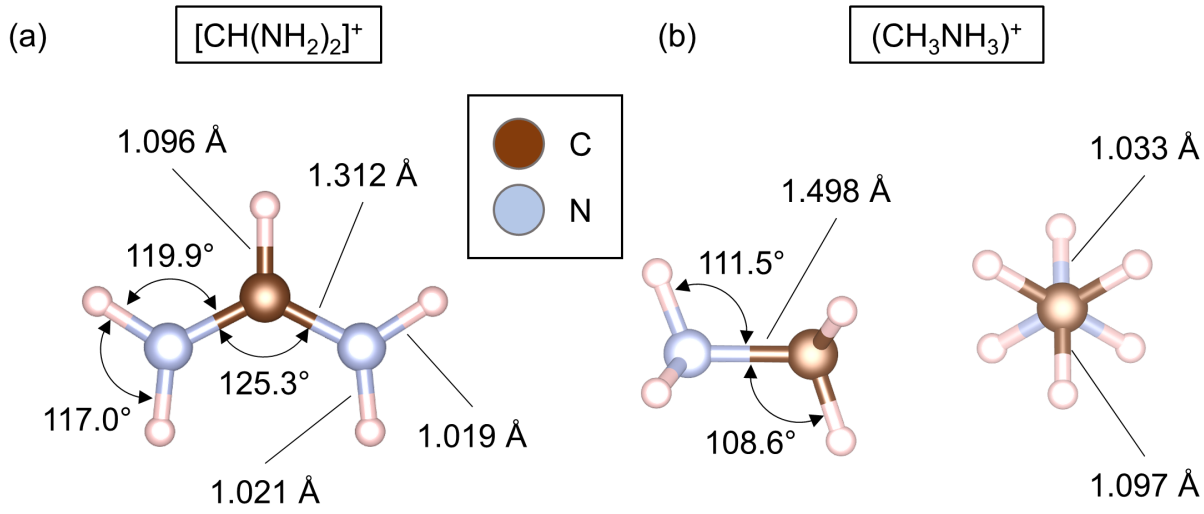

Figure S5: Molecular geometries of (a) $[CH(NH_2)_2]^+$ and (b) $(CH_3NH_3)^+$ from ab initio structural relaxation.

Various structure relaxations were performed to explore plausible hydrogen bonding geometries. Different supercells ($1 \times 1 \times 1$, $\sqrt{2} \times \sqrt{2} \times 1$, $\sqrt{2} \times \sqrt{2} \times 2$, $2 \times 2 \times 2$) allow for different octahedral tilting patterns and orderings of molecular orientation, but differences in the H–acceptor and donor–acceptor distances below varied by only ≈ 0.1 Å. Inclusion or omission of vdW corrections (DFT-D3 method of Grimme)[6] affected relevant distances only by hundredths of Angstroms. Typical hydrogen bonding metrics are presented in the table below, with atom labeling as defined in the following figure. These distances are in excellent agreement with those of the crystallographic database analysis of Steiner for –Nsp^2H$_2$ donors (H–acceptor: 2.79 Å; donor–acceptor: 3.66 Å).[7]

H···acceptor distance	
H1···I1	2.7 Å
H2···I2	2.8 Å
Donor···acceptor distance	
N···I1	3.6 Å
N···I2	3.7 Å

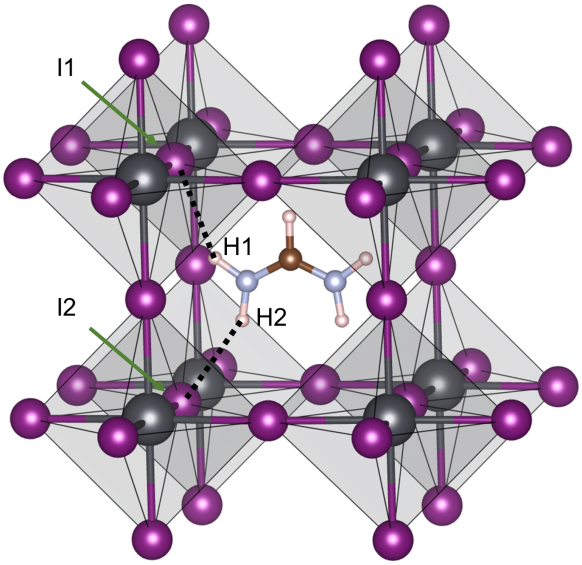

Figure S6: One molecule–cage unit from a typical DFT structure relaxation.

References

(1) Stoumpos, C. C.; Malliakas, C. D.; Kanatzidis, M. G. *Inorg. Chem.* **2013**, *52*, 9019–9038.

(2) Weller, M. T.; Weber, O. J.; Frost, J. M.; Walsh, A. *J. Phys. Chem. Lett.* **2015**, *6*, 3209–3212.

(3) Fabini, D. H.; Stoumpos, C. C.; Laurita, G.; Kaltzoglou, A.; Kontos, A. G.; Falaras, P.; Kanatzidis, M. G.; Seshadri, R. *Angew. Chem. Int. Ed.* **2016**, *55*, 15392–15396.

(4) Chen, T.; Foley, B. J.; Park, C.; Brown, C. M.; Harriger, L. W.; Lee, J.; Ruff, J.; Yoon, M.; Choi, J. J.; Lee, S.-H. *Sci. Adv.* **2016**, *2*, e1601650.

(5) Fabini, D. H.; Hogan, T.; Evans, H. A.; Stoumpos, C. C.; Kanatzidis, M. G.; Seshadri, R. *J. Phys. Chem. Lett.* **2016**, *7*, 376–381.

(6) Grimme, S.; Antony, J.; Ehrlich, S.; Krieg, H. *J. Chem. Phys.* **2010**, *132*, 154104.

(7) Steiner, T. *Acta Crystallogr. Sect. B* **1998**, *54*, 456–463.